

Anisotropic magnetism at the surface of a non-magnetic bulk insulator

Jarryd A. Horn,¹ Keenan E. Avers,¹ Nicholas Crombie,¹ Shanta R. Saha,¹ and Johnpierre Paglione¹

¹*Maryland Quantum Materials Center and Department of Physics,
University of Maryland, College Park, Maryland 20742, USA*

The potential for topological Kondo insulating behavior in d -electron systems has attracted interest in studying the surface states of the correlated insulators FeSb₂ and FeSi. While detailed studies and theoretical description of a spin-orbit coupled ferromagnetic surface state have been applied to FeSi, the magnetic properties of the surface states of FeSb₂ have not been addressed. Here, we report on the surface magnetic properties of FeSb₂, utilizing the surface area dependence of magnetic susceptibility to separate the surface Curie-Weiss temperature dependence from the bulk spin-gap susceptibility. We use these results to further extract the surface magnetic anisotropy of a thin, rough-surfaced single-crystal FeSb₂ to compare with the observed magnetotransport anisotropy, and find good agreement between the anisotropy in the surface magnetization and surface magnetotransport. We conclude with evidence of an anomalous Hall contribution to the low-temperature surface transport.

Topological Kondo insulators (TKIs) such as SmB₆ have become model systems for exploring the interplay between strong electronic correlations and non-trivial band topology [1–4]. In these materials, hybridization between localized $4f$ and itinerant conduction electrons opens a narrow bulk gap at the Fermi level, while symmetry-protected metallic surface states give rise to the characteristic low-temperature resistivity plateau [5]. Following this description, a number of correlated narrow-gap semiconductors based on $3d$ electrons have drawn attention for exhibiting a similar dichotomy of bulk-insulating and surface-conducting behavior [6–10]. Among these, FeSi and FeSb₂ stand out as non-magnetic insulators with extraordinarily robust narrow bulk transport gaps and surface conduction channels at low temperature, prompting comparisons to SmB₆, despite their lack of heavy f -electrons [9].

FeSb₂, in particular, has attracted sustained interest as a narrow-gap correlated semiconductor with remarkable thermoelectric properties [11–13]. Its colossal thermopower at cryogenic temperatures has led to careful studies of its electronic structure which gave rise to its description as a correlated insulator [14, 15]. Spectroscopic measurements have identified fully gapped surface states and a thermally activated spin gap, suggesting a non-topological origin distinct from the Kondo-driven hybridization scenario of SmB₆ [15]. Despite recent theoretical models and experimental evidence, the microscopic origin of these surface states, and their relationship to the bulk electronic and magnetic structure, remains unresolved.

The recent observations of magnetic correlations in the surface electrical transport of FeSb₂ [16] has motivated the comparison to the magnetic surface states of FeSi [17–19], another d -electron system that has been similarly compared to TKIs [20–23]. The evidence of surface magnetism in these materials motivates an interesting fundamental question of whether an intrinsic two-dimensional magnetically ordered surface state could be

stable on the surface of a non-magnetic bulk material such as FeSi or FeSb₂. In two-dimensions, magnetic order is not expected for finite temperatures according to the Mermin-Wagner theorem [24] and has only recently been found in Van der Waals magnets with field induced magnetic anisotropy [25]. To this end, the surface states of FeSi are a curious example of 2D magnetic order, which exists at zero field and finite temperature with minimal crystalline anisotropy [17, 19]. A theoretical description of the surface of FeSi is that of a spin-orbit coupled state formed from dangling bonds, which create a potential gradient normal to the surface associated with the Zak phase [17, 26]. As for FeSb₂, no such theoretical description has been claimed, however, magnetic correlations in the surface magnetotransport properties have been shown to exhibit large anisotropy [16], perhaps large enough to stabilize 2D magnetic order as has been argued for some Van der Waals magnets [25, 27, 28]. Notably, it has been predicted that in RuO₂, the bulk of which is non-magnetic [29], a 2D magnetic surface state may be present by a symmetry breaking [110]-surface reconstruction [30], similar to the mechanism used to describe the metallic surface states in FeSb₂ ARPES results [14]. Furthermore, similar to RuO₂, FeSb₂ is predicted to be an incipient altermagnet with magnetic order expected to be stable with chemical substitution [31] which has motivated recent interests in the electronic structure [32, 33] and inducing magnetic order [34]. In other systems reporting surface magnetism due to surface impurity concentrations induced by surface treatment with no appreciable anisotropy [35].

In this work, we investigate the magnetic properties of the surface conducting states of FeSb₂, extracting the surface magnetic anisotropy and comparing to magnetotransport response. We characterize the surface contribution to the total magnetic susceptibility by measuring the surface area dependence of the magnetization of FeSb₂ powders obtained from systematically repeated grindings, finding that the surface magnetism retains the

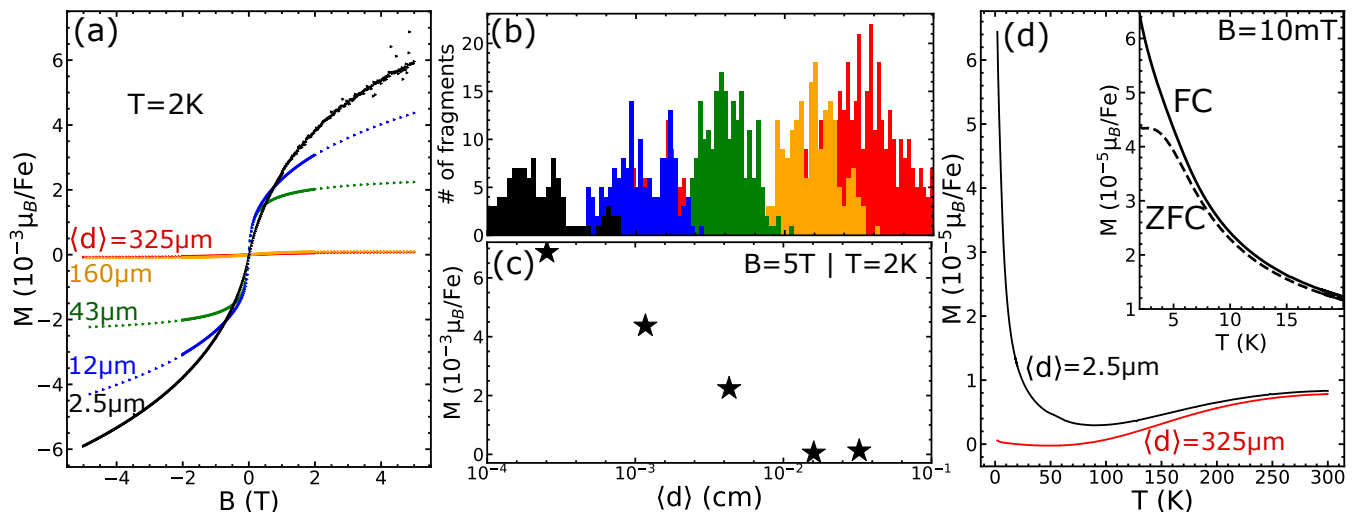


FIG. 1. Magnetization scaling of the powder magnetic susceptibility with surface area (i.e. powder grain size). (a) Magnetization field dependence scaling with each powder step labeled by average diameter. (b) histograms of powder grain size for each powder grind step as calculated from powder images. (c) $B = 5\text{ T}$, $T = 2\text{ K}$ magnetization for each average grain size. (d) M vs T at $B = 10\text{ mT}$ for the most coarse ($\langle d \rangle = 325\mu\text{m}$) and most fine powders with inset for the finest ($\langle d \rangle = 2.5\mu\text{m}$) showing a bifurcation between zero field cooled (ZFC) and field cooled (FC) data.

anisotropy of the bulk crystal structure and is correlated with magnetotransport.

Single crystals of FeSb_2 were synthesized using molten flux method as described in Ref. [6]. Powder fragments for magnetic susceptibility measurements were prepared with a clean ceramic crucible and grain size were measured using Zeiss smart-zoom optical microscope camera and calculated using python scipy toolkit to measure convex hull of individual grains. Measurements of magnetization (M) and magnetic susceptibility ($\chi = \frac{M}{B}$, for small magnetic field, B) as a function of temperature (T) and magnetic field were collected using a Quantum Design MPMS-3 with a gel capsule and straw for powder and quartz rod for single crystal measurements. The gel capsule and straw used for the systematic surface area-dependent measurements were reused to preserve a nearly identical diamagnetic background. We started with a coarsely ground by mortar and pestle sample of FeSb_2 , measured M vs T , M vs B and captured the grain size distribution with microscope images, then further ground the sample and repeated measurements.

The evolution of M vs B , scaled by number of iron atoms determined by mass, increases with subsequent steps as demonstrated in Fig. 1a. Since each step creates smaller and smaller pieces of sample, the surface area per mass increases with each step and therefore Fig. 1a represents M scaling with surface area. From analyzing the powder grain sizes from optical microscope images, we obtain the histogram representation of the average diameter of grains in each measurement step, shown in Fig. 1b, calculated from twice length of average distance from edge to center for each grain. Results from tracking

M at $T = 2\text{ K}$ and $B = 5\text{ T}$ on a log scale in Fig. 1c shows clearly that the $\langle d \rangle = 2.5\mu\text{m}$ magnetization is several orders of magnitude larger than the $\langle d \rangle = 325\mu\text{m}$ magnetization. Fig. 1d compares the fine ($\langle d \rangle = 2.5\mu\text{m}$) and coarse ($\langle d \rangle = 325\mu\text{m}$) magnetization as a function of temperature, showing a bulk M_{bulk} that is proportional to T (consistent with a thermally activated moment [6, 36]) and a surface moment (M_{surface}) that is inversely proportional to T (consistent with free moments [37]). The inset plot of Fig. 1d shows a bifurcation between zero-field cooling (ZFC) and field cooling (FC) data for the fine powder M , which suggests the presence of magnetic order on the surface of FeSb_2 .

Using the results from the fine powder, we are able to assume that the bulk magnetic susceptibility at low temperatures is sufficiently small that we can extract an effective surface magnetic moment (μ_{eff}) using Curie-Weiss fit ($\chi = C/(T - \theta)$ for $\mu_{\text{eff}} = \sqrt{8C}$). To estimate the total surface area, we use the fragments measured by Zeiss Smartzoom microscope as a representative sample and approximate the fragments by prolate spheroids with dimensions given by the minimum and maximum radius of individual fragments. From the Curie-Weiss fits and surface area calculations, we obtain $\mu_{\text{eff}} = 286\mu_B/\text{nm}^2$, which is in fairly good agreement with the results obtained from similar measurements for FeSi powder [19]. The comparison between FeSb_2 powder, FeSi powder and FeSi thin films are given by table I. A possible cause for the disparity between powder and thin film moments is likely to be understood by smooth approximations of spheroids to the fragment shapes. In comparison to a sphere, highly irregular shapes have greater surface ar-

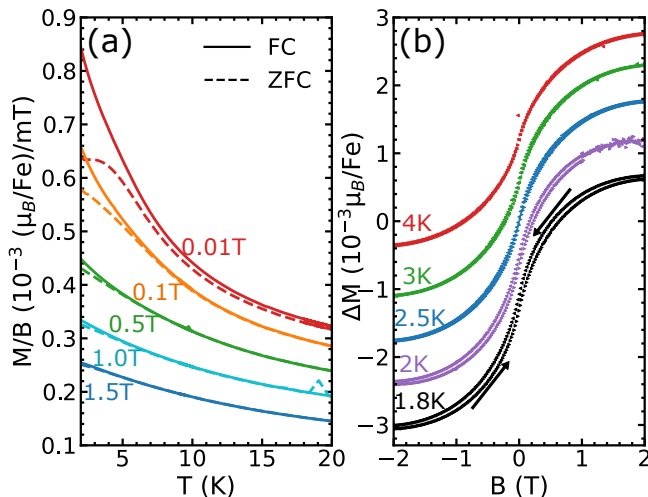


FIG. 2. M/B vs T and magnetization with linear field dependence subtracted for clarity of hysteresis, ΔM vs B , is shown for fine FeSb_2 powder. These results show (a) field dependence of ZFC vs FC bifurcation and (b) temperature dependence of magnetic hysteresis.

TABLE I. Comparison of surface magnetic moment between FeSb_2 and FeSi .

material	M (μ_B/nm^2)	T_c (K)	method
FeSb_2	286	15(5)	powder moment
FeSi [19]	500 (200)	100(20)	powder moment
FeSi [17]	22.5 (12.5)	200	thin film

as by a factor of its sphericity, which can account for a difference of half an order of magnitude in some common shapes [36]. As it stands with $\mu_{eff} = 286 \mu_B/\text{nm}^2$, this would give an effective thickness on the order of tens of unit cells, depending on valence and occupation [37, 38]. This contrasts with the example of calculations for a magnetic surface state in RuO_2 due to surface reconstruction, which gives a 2D localized magnetic surface state with a modest moment of only $3 \mu_B/\text{nm}^2$ [30].

Using the $\langle d \rangle = 2.5 \mu\text{m}$ powder step, we examined the bifurcation from Fig. 1d as a function of magnetic field as shown in Fig. 2a. Traces of a bifurcation between ZFC and FC data disappear between 1 T and 1.5 T field. This is consistent with the results from low temperature M vs B sweeps shown in Fig. 2b, which shows ΔM vs B , where ΔM is the result from subtracting a linear slope from high field data in order to better show the small hysteresis, which closes below 2 T at 1.8 K. The shape of the magnetic hysteresis is unusual for a single phase magnetically ordered system and appears to be “wasps-waisted” (i.e. the hysteresis is narrow at low fields and wider at higher fields), which may be attributed to large magnetocrystalline anisotropy, multiple magnetic phases, or coexisting superparamagnetism [39, 40].

From comparing the coarse (bulk-like) and fine

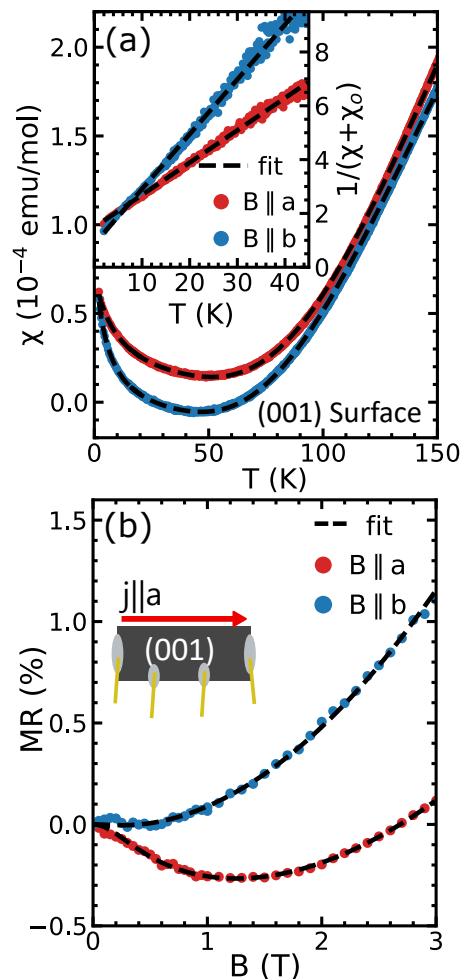


FIG. 3. Anisotropy of surface magnetization compared with surface magnetotransport. (a) magnetic susceptibility of a thin, primarily (001) surface, rough polished single crystal for field along a and b -axes. Dashed line represents a fit, which is a linear combination of bulk spin-gap susceptibility and surface Curie-Weiss susceptibility. (b) Magnetoresistance ($MR = 100\% * (R(B) - R(0))/R(0)$) of a thin, primarily (001) surface sample with current along c -axis and magnetic field along a (red) and b (blue) axes. Dashed line represents fit to linear combination of hopping conduction (positive MR) and magnetic scattering (negative MR).

(surface-like) powder magnetization in Fig. 1, it is clear that the Curie-Weiss M vs T at low temperature may be attributed to the surface magnetism ($\chi_{surface} = \chi_0 + C/(T - \theta)$) and the thermally activated temperature dependent magnetization (increasing with temperature) may be attributed to the bulk magnetism. The bulk magnetization has been described as a spin-gap or Kondo-like behavior [6], with the following expression for the temperature dependence:

$$\chi_{bulk} = \frac{-2N\mu_B^2(1 - \exp(\beta W))}{W(1 + \exp(\beta W))(1 + \exp(\beta(\Delta + W)))}, \quad (1)$$

where N is the number of states, W is the width of density of states bands, which are separated by energy 2Δ and $\beta = 1/kT$. At low temperatures, this gives a vanishingly small moment that is minimally temperature dependent, which is associated with the singlet ground state of the bulk. In this limit, the surface Curie-Weiss behavior is the leading behavior, which is consistent with Fig. 1d and Fig. 3a.

In order to compare the surface magnetization with the observed anisotropic magnetic correlations in the surface magnetotransport [16], we prepared a thin rough (001)-oriented surface (such that field is measured in a - b plane) single-crystal of FeSb₂, less than 0.1 mm thick with silhouette area of 6 mm², which allows us to maximize surface area while maintaining crystal orientation. Since the ratio of surface area to bulk volume is not as large as for a fine powder, the low temperature surface moment is small relative to the high temperature bulk magnetic moment. However, at temperatures below 50 K, the bulk moment is primarily singlet-like and is small relative to the surface magnetic moment. This is clearly shown in the inset of Fig. 3a, which shows a clear Curie-Weiss behavior for which $1/(\chi + \chi_0)$ is linear in T for some χ_0 as shown by good agreement in black dash lined linear fit. Furthermore, we were able to fit the full range of susceptibility to a sum of a Curie-Weiss surface magnetization and a thermally activated bulk magnetization (equation 1) as shown by the dashed lines in the main plot of Fig.3a. In comparing the surface Curie-Weiss behavior for the same (001) surface sample for magnetic field along a and b crystallographic axes, there is a clear magnetic anisotropy present in the low temperature magnetization. Results from Curie-Weiss fits at low temperature (first two results columns of table II) show that the Curie-Weiss effective moment for field along a is approx 30% larger than for field along b along with a Weiss temperature of 12 K for field along a -axis and 4 K for field along b -axis. This comes together to imply a magnetocrystalline anisotropy for which the a -axis is the magnetic easy axis with ferromagnetic correlations.

To compare the surface magnetic anisotropy to the magnetic correlations in the surface magnetotransport properties of the FeSb₂ (001) surface, we prepared a transport sample with current along a -axis and the magnetic field rotating in the a - b plane. In a recent study, we demonstrated that the surface magnetotransport properties of FeSb₂ are independent of the relative alignment of the current and magnetic field [16]. Therefore, in this experiment we should be sensitive only to the magnetocrystalline anisotropy. Instead, the magnetoresistance ($\text{MR}(B) = 100\% * \frac{R(B) - R(0)}{R(0)}$) features a positive MR component due to the effect of the magnetic field on the hopping conduction ($\propto \exp(B)$) and a negative MR component due to the effect of the magnetic field on suppressing magnetic scattering ($\propto -\log(1 + (B/B_0)^2)$). This

TABLE II. Summary of the magnetic anisotropy from fits to magnetic susceptibility (μ_{eff} and θ) and magnetoresistance ($\mu g_0/\alpha$ and $A_1 J\rho_F$).

axes	μ_{eff} (μ_B/Fe)	θ (K)	$\mu g_0/\alpha$ (eV/T)	$A_1 J\rho_F$
a	8.16×10^{-2}	12.4	5.78×10^{-4}	0.134
b	6.27×10^{-2}	4.30	4.84×10^{-4}	0.028

comes together to give a total magnetoresistance:

$$\frac{R(B) - R(0)}{R(0)} = -a \log(1 + b^2 B^2) + \exp(c^2 B^2) - 1 \quad (2)$$

where $a = A_1 J\rho_F$ describes the Kondo coupling between local moments and charge carriers, $b = \frac{g_0 \mu}{\alpha k_B T}$ describes the local moments involved in the scattering process and $c^2 = \frac{te^2 a_{hop}}{\hbar^2 N} \left(\frac{T_{V_{RH}}}{T}\right)^{3/4}$ describes the hopping conduction length-scale, a_{hop} , and site density, N [41, 42].

The (001) surface MR at 2 K fits well to the combined hopping conduction and magnetic scattering model, as evidence from the black dashed fit line shown in Fig. 3b. For field along the b -axis, there is no evidence of magnetic scattering suppression (i.e. MR vs B is monotonically increasing with field), whereas for field along the a -axis, the low field ($B < 2$ T) is dominated by the negative magnetoresistance contribution from suppressing magnetic scattering. This surface magnetotransport anisotropy is qualitatively consistent with the surface magnetization reported in Fig. 3a. Table II compares the results from fitting the magnetoresistance and magnetization data for fields along a and b axes. The relative anisotropy obtained for μ (assuming isotropic g_0/α) is consistent across these fits. Similarly, the anisotropy in the magnetotransport parameter that describes the coupling between charge carriers and local moments (i.e. $A_1 J\rho_F$) is similar to the anisotropy in the Weiss temperature, which describes the coupling strength between moments.

Finally, to complete the study, we examined the low field Hall effect behavior to look for evidence of an anomalous contribution, as reported in FeSi [17, 19]. Understanding the Hall effect in semiconductors with surface states is notoriously challenging due to the strong dependence on surface quality with subsurface cracks from sample preparation playing a large role in the surface transport [43]. To achieve the best surface quality, we used an as-grown facet of FeSb₂, for which the (101) surface is the best candidate as this direction forms large clean surfaces from synthesis. Fig. 4 shows the resistance (Fig. 4a) and Hall effect (Fig. 4b) results for electrical transport on the (101) surface (field along [101] direction) with current along b -axis. The resistance as a function of temperature from Fig. 4a is used to determine the crossover from primarily-bulk to primarily-surface transport regime between 5 K and 10 K. It was

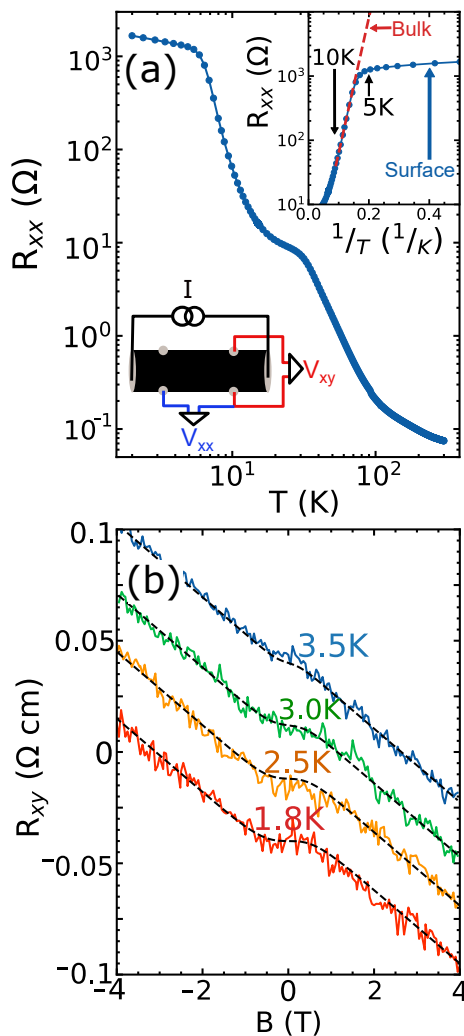


FIG. 4. Hall effect showing some small magnetic correlations in the surface dominated transport regime. (a) resistance vs temperature of primarily (101) surface with current along b -axis. (a, inset) inverse temperature dependence of resistance showing the crossover from primarily bulk electrical conduction around 10 K to primarily surface conduction below 5 K. (b) Hall effect in the primarily surface conduction regime. Dashed line represents linear combination of single channel Hall and anomalous Hall effect component.

previously shown that for this material, the bulk transport properties is characterized by an extraordinarily robust activated behavior, showing no signs of impurity conduction, therefore we assume that the bulk resistance at low temperatures can be predicted by a linear fit to inverse temperature (i.e. $R(T) \propto \exp(T_o/T)$) [9]. The inset of Fig. 4a shows that, using this assumption, at 5 K the bulk of FeSb₂ is several times more resistive than the surface and by 3.5 K, conduction is near entirely through the surface transport channel. Fig. 4b shows that, in the surface transport regime, the Hall effect shows a low field curvature, which increases with decreasing temperature

below 3.5 K. A dashed line fit is used to compare the Hall effect data with a linear and Langevin function combination as to compare with the surface magnetization field dependence for a ferromagnetic contribution. Unfortunately, the Hall mobility is low for the surfaces we've been able to study and therefore this anomalous response is too faint to be able to discern any hysteresis that would be expected for an anomalous Hall effect. Furthermore, we cannot rule out a multi-channel (charge compensated) surface conduction, which would give rise to a non-linear magnetic field dependence in the Hall effect. Therefore, we only point out that this non-linear field dependence, which is shaped like an anomalous Hall contribution, is consistent with the magnetotransport correlations and surface magnetism and provides evidence of an anomalous Hall component in the surface transport properties of FeSb₂.

In summary, we report on the first study of the magnetic properties of the low temperature surface states on FeSb₂. Through systematic study of the magnetization with increasing surface area, we were able to ascribe the observed low temperature Curie-Weiss moment in pure FeSb₂ to moments from the surface states intrinsic to this material. We find also evidence that these surface states are magnetically ordered with a FC/ZFC bifurcation closing around 15 K at 10 mT and magnetic hysteresis. Furthermore, we measure the susceptibility of a flat, high surface-area-to-bulk single crystal for field along a and b crystal axes to find that this surface magnetism retains the anisotropy of the bulk crystal structure, which rules out an isotropic or polycrystalline surface state, which might be expected for a disordered magnetic oxide layer formed on the surface. Additionally, we compare the magnetotransport anisotropy on the same surface and field directions and find good agreement in the anisotropy of the transport and magnetic fit parameters between field along a - and b -axis. The emergence of an anisotropic magnetic surface state in an otherwise nonmagnetic insulator suggests that, although the bulk of FeSb₂ electronic structure is robust against impurities, it remains sensitive to the local symmetry breaking and perturbations at its surfaces. The resulting surface magnetism, which couples strongly to the crystal symmetry, indicates that the nonmagnetic ground state of FeSb₂ lies in close proximity to a magnetic instability. While the surface states in this study exhibit ferromagnetic character, theoretical studies predict a competition between ferromagnetic and altermagnetic order in the bulk. A more detailed examination of the surface perturbations and symmetry breaking mechanisms may offer a pathway toward stabilizing the predicted altermagnetic order.

Research at the University of Maryland was supported by the Gordon and Betty Moore Foundation's EPIQS Initiative Grant No. GBMF9071 (materials synthesis), the U.S. National Science Foundation Grant No. DMR2303090 (sample preparation), the Air Force Office

of Scientific Research Grant No. FA9950-22-1-0023 (experimental measurements), the NIST Center for Neutron Research, and the Maryland Quantum Materials Center.

-
- [1] M. Dzero, J. Xia, V. Galitski, and P. Coleman, *Annu. Rev. Condens. Matter Phys.* **7**, 249 (2016).
- [2] A. Menth, E. Buehler, and T. H. Geballe, *Phys. Rev. Lett.* **22**, 295 (1969).
- [3] R. M. Martin and J. W. Allen, *J. Appl. Phys.* **50**, 7561 (1979).
- [4] S. Rößler, T.-H. Jang, D.-J. Kim, L. H. Tjeng, Z. Fisk, F. Steglich, and S. Wirth, *Proc. Natl. Acad. Sci. U. S. A.* **111**, 4798 (2014).
- [5] Y. S. Eo, A. Rakoski, J. Lucien, D. Mihaliiov, u. Kurdak, P. F. S. Rosa, and Z. Fisk, *Proceedings of the National Academy of Sciences* **116**, 12638–12641 (2019).
- [6] C. Petrovic, Y. Lee, T. Vogt, N. Lazarov, S. Bud’ko, and P. Canfield, *Physical Review B* **72** (2005), 10.1103/physrevb.72.045103.
- [7] K.-J. Xu, S.-D. Chen, Y. He, J. He, S. Tang, C. Jia, E. Yue Ma, S.-K. Mo, D. Lu, M. Hashimoto, T. P. Devereaux, and Z.-X. Shen, *Proceedings of the National Academy of Sciences* **117**, 15409–15413 (2020).
- [8] S. Changdar, S. Aswartham, A. Bose, Y. Kushnirenko, G. Shipunov, N. C. Plumb, M. Shi, A. Narayan, B. Büchner, and S. Thirupathiah, *Physical Review B* **101** (2020), 10.1103/physrevb.101.235105.
- [9] Y. S. Eo, K. Avers, J. A. Horn, H. Yoon, S. R. Saha, A. Suarez, M. S. Fuhrer, and J. Paglione, *Applied Physics Letters* **122** (2023), 10.1063/5.0148249.
- [10] C. Broyles, X. Wan, W. Cheng, D. Wu, H. Tan, Q. Xu, S. L. Gould, H. Siddiquee, L. Xiao, R. Chen, W. Lin, Y. Wu, P. Regmi, Y. S. Eo, J. Liu, Y. Chen, B. Yan, K. Sun, and S. Ran, “High temperature surface state in kondo insulator $U_3Bi_4Ni_3$,” (2025).
- [11] P. Sun, N. Oeschler, S. Johnsen, B. B. Iversen, and F. Steglich, *Phys. Rev. B Condens. Matter Mater. Phys.* **79** (2009).
- [12] H. Zhao, M. Pokharel, G. Zhu, S. Chen, K. Lukas, Q. Jie, C. Opeil, G. Chen, and Z. Ren, *Appl. Phys. Lett.* **99**, 163101 (2011).
- [13] M. Saleemi, M. Y. Tafti, A. Jacquot, M. Jäggle, M. Johnsson, and M. S. Toprak, *Inorganic Chemistry* **55**, 1831 (2016), pMID: 26836130, <https://doi.org/10.1021/acs.inorgchem.5b02658>.
- [14] A. Chikina, J.-Z. Ma, W. H. Brito, S. Choi, P. Sémon, A. Kutepov, Q. Du, J. Jandke, H. Liu, N. C. Plumb, M. Shi, C. Petrovic, M. Radovic, and G. Kotliar, *Physical Review Research* **2** (2020), 10.1103/physrevresearch.2.023190.
- [15] H. Li, G. Wang, N. Ding, Q. Ren, G. Zhao, W. Lin, J. Yang, W. Yan, Q. Li, R. Yang, S. Yuan, J. D. Denlinger, Z. Wang, X. Zhang, L. A. Wray, S. Dong, D. Qian, and L. Miao, *Proceedings of the National Academy of Sciences* **121** (2024), 10.1073/pnas.2321193121.
- [16] J. A. Horn, Y. S. Eo, K. Avers, H. Yoon, R. G. Dorman, S. R. Saha, and J. Paglione, (2025), arXiv:2509.05788.
- [17] Y. Ohtsuka, N. Kanazawa, M. Hirayama, A. Matsui, T. Nomoto, R. Arita, T. Nakajima, T. Hanashima, V. Ukleev, H. Aoki, M. Mogi, K. Fujiwara, A. Tsukazaki, M. Ichikawa, M. Kawasaki, and Y. Tokura, *Science Advances* **7** (2021), 10.1126/sciadv.abj0498.
- [18] Y. Deng, Y. Yan, H. Wang, E. Lee-Wong, C. M. Moir, Y. Fang, W. Xie, and M. B. Maple, *Physical Review B* **108** (2023), 10.1103/physrevb.108.115158.
- [19] K. E. Avers, Y. S. Eo, H. Yoon, J. A. Horn, S. R. Saha, A. Suarez, P. Zavalij, and J. Paglione, *Phys. Rev. B.* **110** (2024).
- [20] Y. Fang, S. Ran, W. Xie, S. Wang, Y. S. Meng, and M. B. Maple, *Proceedings of the National Academy of Sciences* **115**, 8558–8562 (2018).
- [21] C. Fu, M. P. C. M. Krijn, and S. Doniach, *Physical Review B* **49**, 2219–2222 (1994).
- [22] Z. Schlesinger, Z. Fisk, H.-T. Zhang, and M. B. Maple, *Physica B Condens. Matter* **237-238**, 460 (1997).
- [23] A. J. Breindel, Y. Deng, C. M. Moir, Y. Fang, S. Ran, H. Lou, S. Li, Q. Zeng, L. Shu, C. T. Wolowiec, I. K. Schuller, P. F. S. Rosa, Z. Fisk, J. Singleton, and M. B. Maple, *Proc. Natl. Acad. Sci. U. S. A.* **120**, e2216367120 (2023).
- [24] N. D. Mermin and H. Wagner, *Physical Review Letters* **17**, 1133–1136 (1966).
- [25] C. Gong, L. Li, Z. Li, H. Ji, A. Stern, Y. Xia, T. Cao, W. Bao, C. Wang, Y. Wang, Z. Q. Qiu, R. J. Cava, S. G. Louie, J. Xia, and X. Zhang, *Nature* **546**, 265–269 (2017).
- [26] J. Zak, *Physical Review Letters* **62**, 2747–2750 (1989).
- [27] F. Xiao and Q. Tong, *Nano Letters* **22**, 3946–3952 (2022).
- [28] R. H. Aguilera-del Toro, M. Arruabarrena, A. Leonardo, and A. Ayuela, *Nanoscale Advances* **5**, 2813–2819 (2023).
- [29] L. Kiefer, F. Wirth, A. Bertin, P. Becker, L. Bohaty, K. Schmalzl, A. Stunault, J. A. Rodriguez-Velamazán, O. Fabelo, and M. Braden, *J. Phys. Condens. Matter* **37**, 135801 (2025).
- [30] D. Q. Ho, D. Q. To, R. Hu, G. W. Bryant, and A. Janotti, “Symmetry-breaking induced surface magnetization in non-magnetic ruo_2 ,” (2025).
- [31] I. I. Mazin, K. Koepf, M. D. Johannes, R. González-Hernández, and L. Šmejkal, *Proceedings of the National Academy of Sciences* **118** (2021), 10.1073/pnas.2108924118.
- [32] C. Phillips, G. Pokharel, K. Shtefiienko, S. R. Bhandari, D. E. Graf, D. P. Rai, and K. Shrestha, *Physical Review B* **111** (2025), 10.1103/physrevb.111.075141.
- [33] A. Gauswami and P. K. Jha, *Journal of Physics: Condensed Matter* **37**, 305801 (2025).
- [34] S. R. Bhandari, R. Tamang, K. Shrestha, S. Brahim, S. Lounis, and D. P. Rai, (2025), arXiv:2507.22018.
- [35] J. M. D. Coey, M. Venkatesan, and P. Stamenov, *Journal of Physics: Condensed Matter* **28**, 485001 (2016).
- [36] T. Li, S. Li, J. Zhao, P. Lu, and L. Meng, *Particuology* **10**, 97–104 (2012).
- [37] S. Mugiraneza and A. M. Hallas, *Communications Physics* **5** (2022), 10.1038/s42005-022-00853-y.
- [38] P. Villars and K. Cenzual, “FeSb₂ crystal structure: Datashet from springer materials,”.
- [39] A. P. Roberts, Y. Cui, and K. L. Verosub, *J. Geophys. Res.* **100**, 17909 (1995).
- [40] T. Magno de Lima Alves, B. F. Amorim, M. A. Morales Torres, C. G. Bezerra, S. Nóbrega de Medeiros, P. L. Gastelois, L. E. Fernandez Outon, and W. Augusto de Almeida Macedo, *RSC Adv.* **7**, 22187 (2017).
- [41] R. P. Khosla and J. R. Fischer, *Physical Review B* **2**, 4084–4097 (1970).

- [42] B. I. Shklovskii and A. L. Efros, “Electronic properties of doped semiconductors,” (Springer Berlin Heidelberg, 1984) Chap. 9, pp. 202–212.
- [43] Y. S. Eo, S. Wolgast, A. Rakoski, D. Mihaliov, B. Y. Kang, M. S. Song, B. K. Cho, M. C. Hatnean, G. Balakrishnan, Z. Fisk, S. R. Saha, X. Wang, J. Paglione, and u. Kurdak, *Physical Review B* **101** (2020), 10.1103/physrevb.101.155109.